

# 2D chemical evolution model: the impact of galactic disc asymmetries on azimuthal chemical abundance variations

E. Spitoni<sup>1</sup> <sup>\*</sup>, G. Cescutti<sup>2</sup>, I. Minchev<sup>3</sup>, F. Matteucci<sup>2,4</sup>, V. Silva Aguirre<sup>1</sup>,  
M. Martig<sup>5</sup>, G. Bono<sup>6,7</sup>, and C. Chiappini<sup>3</sup>

<sup>1</sup> Stellar Astrophysics Centre, Department of Physics and Astronomy, Aarhus University, Ny Munkegade 120, DK-8000 Aarhus C

<sup>2</sup> I.N.A.F. Osservatorio Astronomico di Trieste, via G.B. Tiepolo 11, 34131, Trieste, Italy

<sup>3</sup> Leibniz-Institut für Astrophysik Potsdam, An der Sternwarte 16, 14482, Potsdam, Germany

<sup>4</sup> Dipartimento di Fisica, Sezione di Astronomia, Università di Trieste, Via G. B. Tiepolo 11, I-34143 Trieste, Italy

<sup>5</sup> Astrophysics Research Institute, Liverpool John Moores University, 146 Brownlow Hill, Liverpool L3 5RF, UK

<sup>6</sup> Dipartimento di Fisica, Università di Roma Tor Vergata, via della Ricerca Scientifica 1, I-00133 Rome, Italy

<sup>7</sup> I.N.A.F. Osservatorio Astronomico di Roma, Via Frascati 33, 00078 Monte Porzio Catone, Italy

Received xxxx / Accepted xxxx

## ABSTRACT

**Context.** Galactic disc chemical evolution models generally ignore azimuthal surface density variation that can introduce chemical abundance azimuthal gradients. Recent observations, however, have revealed chemical abundance changes with azimuth in the gas and stellar components of both the Milky Way and external galaxies.

**Aims.** To quantify the effects of spiral arm density fluctuations on the azimuthal variations of the oxygen and iron abundances in disc galaxies.

**Methods.** We develop a new 2D galactic disc chemical evolution model, capable of following not just radial but also azimuthal inhomogeneities.

**Results.** The density fluctuations resulting from a Milky Way-like N-body disc formation simulation produce azimuthal variations in the oxygen abundance gradients of the order of 0.1 dex. Moreover, in agreement with the most recent observations in external galaxies, the azimuthal variations are more evident in the outer galactic regions. Using a simple analytical model, we show that the largest fluctuations with azimuth result near the spiral structure corotation resonance, where the relative speed between spiral and gaseous disc is the slowest.

**Conclusions.** We provided a new 2D chemical evolution model capable of following azimuthal density variations. Density fluctuations extracted from a Milky Way-like dynamical model lead to a scatter in the azimuthal variations of the oxygen abundance gradient in agreement with observations in external galaxies. We interpret the presence of azimuthal scatter at all radii by the presence of multiple spiral modes moving at different pattern speeds, as found in both observations and numerical simulations.

**Key words.** Galaxy: evolution, disc – stars: abundances – ISM: abundances

## 1. Introduction

In recent years, integral field spectrographs (IFSs) have largely substituted long-slit spectrographs in studies designed to characterize the abundance distribution of chemical elements in external galaxies. IFSs have permitted for the first time to measure abundances throughout the entire two-dimensional extent of a galaxy (or a large part thereof) and, thus, to detect azimuthal and radial trends (Vogt et al. 2017).

In the last years, several observational works have been found evidence of significant azimuthal variations in the abundance gradients in external galaxies. Sánchez et al. (2015) and Sánchez-Menguiano et al. (2016) analyzed in detail the chemical inhomogeneities of the external galaxy NGC 6754 with the Multi Unit Spectroscopic Explorer (MUSE), concluding that

the azimuthal variations of the oxygen abundances are more evident in the external part of the considered galaxy.

Vogt et al. (2017) studied the galaxy HCG 91c with MUSE and arrived to the conclusion that the enrichment of the interstellar medium has proceeded preferentially along spiral structures, and less efficiently across them.

Azimuthal variations have been detected in the oxygen abundance also in the external galaxy M101 by Li et al. (2013). Ho et al. (2017) presented the spatial distribution of oxygen in the nearby spiral galaxy NGC 1365. This galaxy is characterized by a negative abundance gradient for oxygen along the disc, but systematic azimuthal variations of  $\sim 0.2$  dex occur over a wide radial range of galactic radii and peak at the two spiral arms in NGC 1365. In the same work, the authors presented a simple chemical evolution model to reproduce the observations. Azimuthal variations can be explained by two physical processes: after a local self enrichment phase in the inter-

<sup>\*</sup> email to: spitoni@phys.au.dk

arm region, a consequent mixing and dilution phase is dominant on larger scale (kpc scale) when the spiral density waves pass through.

Probing azimuthal inhomogeneities of chemical abundances has been attempted in the Milky Way system too. Balser et al. (2011), measuring H II region oxygen abundances, found that the slopes of the gradients differ by a factor of two in their three Galactic azimuth angle bins. Moreover, significant local iron abundance inhomogeneities have also been observed with Galactic Cepheids (Pedicelli et al. 2009; Genovali et al. 2014).

Balser et al. (2015) underlined the importance of azimuthal metallicity structure in the Milky Way disc making for the first time radio recombination line and continuum measurements of 21 HII regions located between Galactic azimuth  $\phi=90^\circ$  -  $130^\circ$ . The radial gradient in [O/H] is  $-0.082 \pm 0.014$  dex  $\text{kpc}^{-1}$  for  $\phi=90^\circ$  -  $130^\circ$ , about a factor of 2 higher than the average value between  $\phi=0^\circ$  -  $60^\circ$ . It was suggested that this may be due to radial mixing from the Galactic Bar.

Analyzing the Scutum Red-Supergiant (RSG) clusters at the end of the Galactic Bar, Davies et al. (2009) concluded that a simple one-dimensional parameterisation of the Galaxy abundance patterns is insufficient at low Galactocentric distances, as large azimuthal variations may be present. Combining these results with other data in the literature points towards large-scale ( $\sim$  kpc) azimuthal variations in abundances at Galactocentric distances of 3-5 kpc. It thus appears that the usual approximation of chemical evolution models assuming instantaneous mixing of metallicity in the azimuthal direction is unsubstantiated.

Azimuthal abundance gradients due to radial migration in the vicinity of spiral arms in a cosmological context have been studied in detail by Grand et al. (2012, 2014, 2016), and Sánchez-Menguiano et al. (2016).

Alternatively, Khoperskov et al. (2018) investigated the formation of azimuthal metallicity variations in the discs of spiral galaxies in the absence of initial radial metallicity gradients. Using high-resolution N-body simulations, they modeled composite stellar discs, made of kinematically cold and hot stellar populations, and study their response to spiral arm perturbations. They found that azimuthal variations in the mean metallicity of stars across a spiral galaxy are not necessarily a consequence of the reshaping, by radial migration, of an initial radial metallicity gradient. They indeed arise naturally also in stellar discs which have initially only a negative vertical metallicity gradient.

The aim of this paper is to develop a detailed 2D galactic disc chemical evolution model, able to follow the evolution of several chemical elements as in previous 1D models, but also taking into account azimuthal surface density variations. In this paper when we refer to the thin and thick discs we mean the low- and high- $[\alpha/\text{Fe}]$  sequences in the  $[\alpha/\text{Fe}]$ - $[\text{Fe}/\text{H}]$  plane. Defining the thin and thick discs morphologically, rather than chemically, identifies a mixture of stars from both the low- and high- $[\alpha/\text{Fe}]$  sequences, and vice versa (Minchev et al. 2015, Martig et al. 2016). It is, therefore, very important to make this distinction and avoid confusion. We follow the chemical evolution of the thin disk component, i.e. the low- $\alpha$  population. We assume that the oldest stars of that low- $\alpha$  component are asso-

ciated with ages of  $\sim 11$  Gyr, in agreement with asteroseismic age estimates (Silva Aguirre et al. 2018).

Starting from the classical 1D Matteucci & François (1989) approach (the Galactic disc is assumed to be formed by an infall of primordial gas) we included 2D surface density fluctuation in the Milky Way disc chemo-dynamical model by Minchev et al. (2013) (hereafter MCM13), as well as using analytical spiral arm prescriptions.

Our paper is organized as follows. In Section 2, we describe the framework used for the new model. In Section 2.1 the adopted nucleosynthesis prescriptions are reported. In Section 2.2 the density fluctuation from the chemo-dynamical model by MCM13 are indicated. In Section 2.3 we present the analytical expressions for the density perturbations due to Galactic spiral arm. In Section 3 we present our results with the density fluctuation from chemo-dynamical models and with an analytical spiral arm prescription are reported. Finally, our conclusions are drawn in Section 4.

## 2. A 2D galactic disc chemical evolution model

The basis for the 2D chemical evolution model we develop in this section is the classical 1D Matteucci & François (1989) approach, in which the Galactic disc is assumed to be formed by an infall of primordial gas. The infall rate for the thin disc (the low- $\alpha$  sequence) of a certain element  $i$  at the time  $t$  and Galactocentric distance  $R$  is defined as:

$$B(R, t, i) = X_{A_i} b(R) e^{-\frac{t}{\tau_D(R)}}, \quad (1)$$

where  $X_{A_i}$  is the abundance by mass of the element  $i$  of the infall gas that here is assumed to be primordial, while the quantity  $\tau_D(R)$  is the time-scale of gas accretion. The coefficient  $b(R)$  is constrained by imposing a fit to the observed current total surface mass density  $\Sigma_D$  in the thin disc as a function of the Galactocentric distance given by:

$$\Sigma_D(R, t_G) = \Sigma_{D,0} e^{-R/R_D}, \quad (2)$$

where  $t_G$  is the present time,  $\Sigma_{D,0}$  is the central total surface mass density and  $R_D$  is the disc scale length. The fit of the  $\Sigma_D(R)$  quantity using the infall rate law of eq. (1) is given by:

$$\sum_i \int_0^{t_G} X_{A_i} b(R) e^{-\frac{t}{\tau_D(R)}} dt = \Sigma_D(R, t_G), \quad (3)$$

The observed total disc surface mass density in the solar neighbourhood is  $\Sigma_D(8 \text{ kpc}, t_G) = 54 \text{ M}_\odot \text{ pc}^{-2}$  (see Romano et al. 2000 for a discussion of the choice of this surface density). The infall rate of gas that follows an exponential law is a fundamental assumption adopted in most of the detailed numerical chemical evolution models in which the instantaneous recycling approximation (IRA) is relaxed.

An important ingredient to reproduce the observed radial abundance gradients along the Galactic disc is the inside-out formation on the disc (Spitoni & Matteucci 2011, Cescutti et al. 2007, Mott et al. 2013). The timescale  $\tau_D(R)$  for the mass accretion is assumed to increase with the Galactic radius following a linear relation given by (see Chiappini et al. 2001):

$$\tau_D(R) = 1.033R(\text{kpc}) - 1.27 \text{ Gyr} \quad (4)$$

for Galactocentric distances  $\geq 4$  kpc. For the star formation rate (SFR) we adopt a Kennicutt (1998) law proportional to the gas surface density:

$$\Psi(R, t) = \nu \Sigma_g^k(R, t), \quad (5)$$

where  $\nu$  is the star formation efficiency (SFE) process and  $\Sigma_g(R, t)$  is the gas surface density at a given position and time. The exponent  $k$  is fixed to 1.5 (see Kennicutt 1998).

We divide the disc into concentric shells 1 kpc wide in the radial direction. Each shell is itself divided into 36 segments of width  $10^\circ$ . Therefore at a fixed Galactocentric distance 36 zones have been created.

With this new configuration we can take into account variations of the SFR along the annular region, produced by density perturbations driven by spiral arms or bars. Therefore, an azimuthal dependence appears in eq. (5) and, which can be written as follows:

$$\Psi(R, t, \phi) = \nu \Sigma_g^k(R, t, \phi). \quad (6)$$

In this paper we will show results related to the effects of density fluctuations of the chemo-dynamical model of MCM13 and we will test the effects of an analytical formulation for the density perturbations created by spiral arm waves. The reference model without any density azimuthal perturbation is similar to the one by Cescutti et al. (2007), which as been shown to be quite successful in reproducing the most recent abundance gradients observed in Cepheids (Genovali et al. 2015).

### 2.1. Nucleosynthesis prescriptions

In this work we present results for the azimuthal variations of abundance gradients for oxygen and iron. As done in a number of chemical evolution models in the past (e.g. Cescutti et al. 2006, Spitoni et al. 2015, 2019, Vincenzo et al. 2019), we adopt the nucleosynthesis prescriptions by François et al. (2004) who provided theoretical predictions of [element/Fe]-[Fe/H] trends in the solar neighbourhood for 12 chemical elements.

François et al. (2004) selected the best sets of yields required to best fit the data (details related to the observational data collection are in François et al. 2004). In particular, for the yields of Type II SNe they found that the Woosley & Weaver (1995) ones provide the best fit to the data: no modifications are required for the yields of iron, as computed for solar chemical composition, whereas for oxygen, the best results are given by yields computed as functions of the metallicity. The theoretical yields by Iwamoto et al. (1999) are adopted for the Type SNeIa, and the prescription for single low-intermediate mass stars is by van den Hoek & Groenewegen (1997).

Although François et al. (2004) prescriptions still provide reliable yields for several elements, we must be cautious about oxygen. Recent results have shown that rotation can influence the oxygen nucleosynthesis in massive stars (Meynet & Meader 2002) and therefore chemical evolution (Cescutti & Chiappini 2010), in particular at low metallicity. However, this does not affects our results being the data shown in this project relatively metal rich. Moreover, we are mostly interested in differential effects, rather than absolute values.

### 2.2. 2D disc surface density fluctuations from the MCM13 model

We consider the gas density fluctuations present in the Milky Way like simulation obtained by Martig et al. (2012) and chosen in MCM13 for their chemodynamical model. The simulated galaxy has a number of properties consistent with the Milky Way, including a central bar. MCM13 followed the disc evolution for a time period of about 11 Gyr, which is close to the age of the oldest low- $\alpha$  disc stars in the Milky Way. The classical 1D chemical evolution model is quite successful in reproducing abundance gradient along the Galactic disc (Cescutti et al. 2007).

The chemical evolution model used by MCM13 was very similar to the one adopted here; a comparison between its star formation history and that of the simulation was presented in Fig. A.1 by Minchev et al. (2014), showing good agreement. To extract the gas density variations we binned the disk into 18 1-kpc-wide radial bins and  $10^\circ$ -wide azimuthal bins at  $|z| < 1$  kpc. The time resolution is 37.5 Myr for 11 Gyr of evolution. All of the above is used for our new model described below.

With the aim of preserving the general trend of the 1D chemical evolution model, we introduce a density contrast function  $f$  related to the perturbations originated by the MCM13 model. At a fixed Galactocentric distance  $R$ , time  $t$  and azimuthal coordinate  $\phi$ , the new surface mass density is:

$$\Sigma_D(R, t, \phi) = \Sigma_D(R, t) f(\phi, R, t). \quad (7)$$

We impose that the average value of the density contrast  $f$  is 1, i.e.:

$$\langle f(\phi, R, t) \rangle_\phi = 1. \quad (8)$$

This guarantees that, at a fixed Galactocentric distance  $R$  and a time  $t$ , the average surface mass density is the one predicted by the 1 D chemical evolution model.

### 2.3. ISM density fluctuations from analytical spiral structure

Here we investigate the effect of an analytical spiral arm formulation on the azimuthal variations of the abundance gradients.

In particular, we analyse steady wave spiral patterns. As suggested by Bertin et al (1989) and Lin & Shu (1966) when the number of important spiral modes of oscillation is small, the spiral structure is expected to have a highly regular grand design and to evolve in time in a quasi-stationary manner.

In this work, we consider the model presented by Cox & Gómez (2002). The expression for the time evolution of the density perturbation created by spiral arms, referred to an inertial reference frame not corotating with the Galactic disk, in terms of the surface mass density is:

$$\Sigma_S(R, \phi, t) = \chi(R, t_G) M(\gamma), \quad (9)$$

where  $\chi(R, t_G)$  is the present day amplitude of the spiral density:

$$\chi(R, t_G) = \Sigma_{S,0} e^{-\frac{R-R_0}{R_S}}, \quad (10)$$

while  $M(\gamma)$  is the modulation function for the “concentrated arms” given by Cox & Gómez (2002). The  $M(\gamma)$  function can be expressed as follows:

$$M(\gamma) = \left( \frac{8}{3\pi} \cos(\gamma) + \frac{1}{2} \cos(2\gamma) + \frac{8}{15\pi} \cos(3\gamma) \right), \quad (11)$$

$$\gamma(R, \phi, t) = m \left[ \phi + \Omega_s t - \phi_p(R_0) - \frac{\ln(R/R_0)}{\tan(\alpha)} \right]. \quad (12)$$

In eq. (12),  $m$  is the number of spiral arms,  $\alpha$  is the pitch angle,  $R_S$  is the radial scale-length of the drop-off in density amplitude of the arms,  $\Sigma_0$  is the surface arm density at fiducial radius  $R_0$ ,  $\Omega_s$  is the pattern angular velocity, with the azimuthal coordinate  $\phi$  increasing counter-clockwise and a clockwise rotation,  $\phi_p(R_0)$  is the coordinate  $\phi$  computed at  $t=0$  Gyr and  $R_0$ . An important feature of such a perturbation is that its average density at a fixed Galactocentric distance  $R$  and time  $t$  is zero,

$$\langle \Sigma_S \rangle_\phi = \Sigma_{S,0} e^{-\frac{R-R_0}{R_S}} \langle M(\gamma) \rangle_\phi = 0. \quad (13)$$

In Fig. 1 we show the modulation function  $M(\gamma)$  of “concentrated arms” on the Galactic plane using the model parameters suggested by Cox & Gómez (2002):  $R_0 = 8$  kpc,  $\alpha = 15^\circ$ ,  $R_S = 7$  kpc. The modulation function is computed at 5 Gyr assuming the angular velocity value of  $\Omega_s = 20$  km s<sup>-1</sup> kpc<sup>-1</sup> and  $\phi_p(R_0) = 0$ . In this work we aim to investigate the effects of spiral arm density perturbations on the chemical enrichment by ejecta from stellar populations perfectly corotating with the Galactic disk. Our purpose here is the study of regular gas density perturbation linked to simple but reliable spiral arm descriptions.

To properly describe the temporal evolution of local density perturbations, the relative spiral arm speed pattern compared to the Galactic disk motion must be computed (further details will be provided in Section 3.2, in the Result discussion).

Cox & Gómez (2002) provided a value for the spiral arm perturbation density at 8 kpc equal to  $\rho_0 = \frac{14}{11} \text{ m}_H \text{ cm}^{-3}$ . Our implementation requires the surface density  $\Sigma_{S,0}$ , which can be recovered from the  $z$  direction amplitude provided by Cox & Gómez (2002) (their eq. 1), with the following relation:

$$\Sigma_{S,0} = 2\rho_0 \int_0^\infty \text{sech}^2\left(\frac{x}{H}\right) dx = 2H\rho_0, \quad (14)$$

where  $H$  is the disc scale-height. Adopting  $H=180$  pc (chosen to match the scale-height of the thin stellar disc proposed by Dehnen & Binney 1998, Model2; and in agreement with Spitoni et al. 2008) we obtain

$$\Sigma_{S,0} = 21.16 \text{ M}_\odot \text{ pc}^{-2}. \quad (15)$$

It is important to underline that in our approach the time dependence of the density perturbation by the spiral arms is only in the modulation function  $M(\gamma)$  through the term  $\Omega_s t$  (see eqs. 11 and 12). Currently, there are no analytical prescriptions for the time evolution of both the amplitude of the spiral arm perturbation and its radial profile in the Galactic evolution context (spiral arm redshift evolution). Therefore, we make the reasonable assumption that during the Galactic evolution

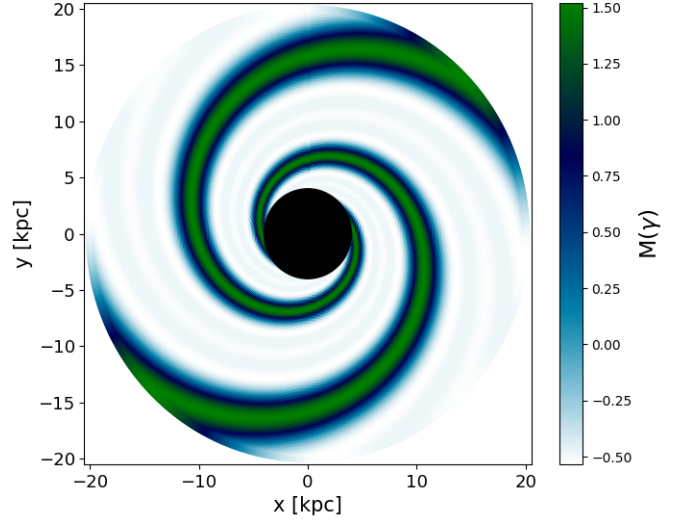


**Fig. 1.** The modulation function  $M(\gamma)$  of eq. (11) for concentrated arms by Cox & Gómez (2002) with  $N = 2$  spiral arms, fiducial radius  $R_0 = 8$  kpc, pitch angle  $\alpha = 15^\circ$ , and  $\phi_p(R_0) = 0$ .

the ratio between the amplitude of the spiral density perturbation  $\chi(R, t)$  and the total surface density  $\Sigma_D(R, t)$  computed at the same Galactocentric distance  $R$  remains constant in time, i.e.  $\frac{d}{dt} [\chi(R, t)/\Sigma_D(R, t)] = 0$ , assuming a coeval evolution of these two structures in time. We define the dimensionless quantity  $\delta_S(R, \phi, t)$  as the following ratio:

$$\delta_S(R, \phi, t) = \frac{\Sigma_S(R, \phi, t) + \Sigma_D(R, t)}{\Sigma_D(R, t)} = 1 + \frac{\Sigma_S(R, \phi, t)}{\Sigma_D(R, t)}. \quad (16)$$

With the assumption that the ratio  $\chi(R, t)/\Sigma_D(R, t)$  is constant in time, eq. (16) becomes:

$$\delta_S(R, \phi, t) = 1 + M(\gamma) \frac{\chi(R, t_G)}{\Sigma_D(R, t_G)}. \quad (17)$$

If we include the contribution of the perturbation originated by spiral arm in the SFR driven by a linear Schmidt (1959) law (i.e.  $\Psi = \nu \Sigma_g(R, t)$ ) we have that:

$$\Psi(R, t, \phi)_{d+s} = \nu \Sigma_g(R, t) \delta_S(R, \phi, t). \quad (18)$$

We are aware that this is a simplification to the more complex behavior seen in N-body simulations (Quillen et al. 2011, Minchev et al. 2012b, Sellwood and Carlberg 2014) and external galaxies (Elmegreen et al. 1992; Rix & Zaritsky 1995; Meidt et al. 2009), where multiple spiral patterns have been found. We will make use of this description in Section 3.2.2, where we will consider the simultaneous perturbation by a number of spiral patterns moving at different angular velocities.

As stated in the previous Section, the average modulation function over the azimuth  $\phi$  at a fixed time  $t$  and Galactocentric distance  $R$  is null ( $\langle M(\gamma) \rangle_\phi = 0$ ). Therefore, in presence of a linear Schmidt (1959) law at a fixed Galactocentric distance the average value of  $\Psi(R, t, \phi)_{d+s}$  over  $\phi$  of the SFR defined

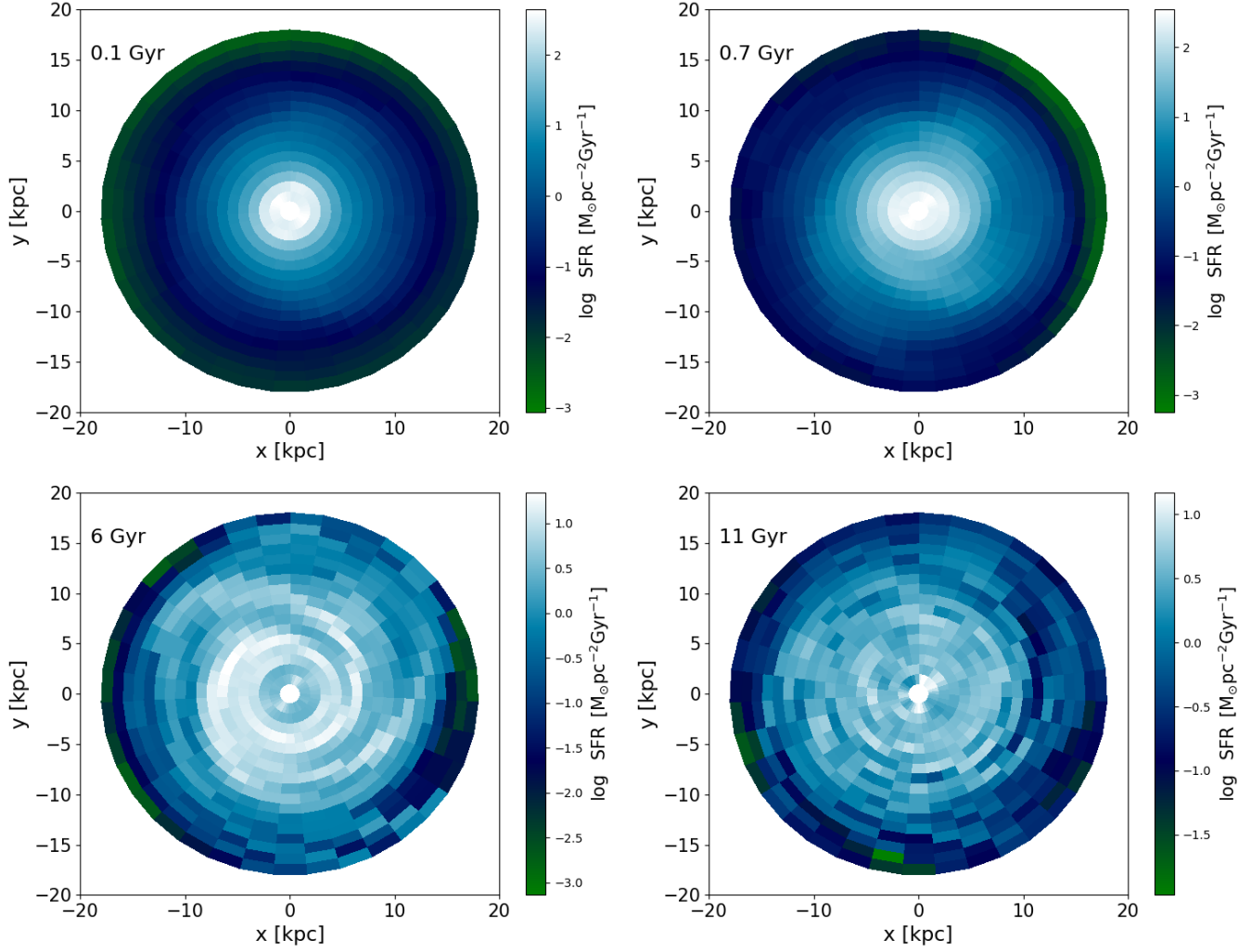


**Fig. 2.** The galactic disc SFR in units of  $M_{\odot} \text{ pc}^{-2} \text{ Gyr}^{-1}$  computed at 0.1, 0.7, 6, 11 Gyr after the start of disc formation, for the chemical evolution model in which we tested the effects of the density fluctuations resulting from the MCM13 model.

in eq. (18) is equal to the unperturbed SFR by the following expression:

$$\begin{aligned} \langle \Psi(R, t, \phi)_{d+s} \rangle_{\phi} &= \Psi(R, t) \langle 1 + M(\gamma) \frac{\chi(R)}{\Sigma_D(R, t_G)} \rangle_{\phi} = \\ &= \Psi(R, t) \left( 1 + \langle M(\gamma) \rangle_{\phi} \frac{\chi(R)}{\Sigma_D(R, t_G)} \right) = \Psi(R, t). \end{aligned} \quad (19)$$

Here, we do not adopt a linear Schmidt (1959) law, and we use the SFR proposed by Kennicutt (1998) which exhibits the exponent  $k=1.5$ . Hence, the SFR in the Galactic disc in presence of spiral arm density perturbations becomes:

$$\Psi_k(R, t, \phi)_{d+s} = \nu \Sigma_g(R, t)^k \delta_S(R, \phi, t)^k. \quad (20)$$

Roberts (1969) provided the exact shape of the steady gas distribution in spiral arms, finding an offset between the maximum of the stellar spiral arm and the maximum of the gas distribution driven by galactic shocks. In his Figure 7, it is shown that the regions of newly born luminous stars and the HII regions lie on the inner side of the observable gaseous spiral arm

of HI. The presence of a small but noticeable offset between the gas and stellar spiral arms has been also found in the study of interactions between disc galaxies and perturbing companions in 3D N-body/smoothed hydrodynamical numerical simulations by Pettitt (2006).

Because of uncertainties related to the real magnitude of this offset (small offsets are predicted by Pettitt 2006), in our work we do not consider it, and the SFR is more enhanced in correspondence of the total density perturbation peak (see eq. 17 and the modulation function in Figure 1). We are aware that is true only near the corotation radius, however with our simpler approach we provide an upper limit estimate for the azimuthal abundance variations generated by steady spiral arms density perturbations. In presence of an off-set the density perturbation should be less “concentrated” and more smeared.

Our model in the presence of analytical spiral arms must be considered as a first attempt to include spiral structure in a classical chemical evolution model. As stated in Section 2.2, we will also present results for the azimuthal abundance variations originated by chemodynamical Milky Way like simulation in

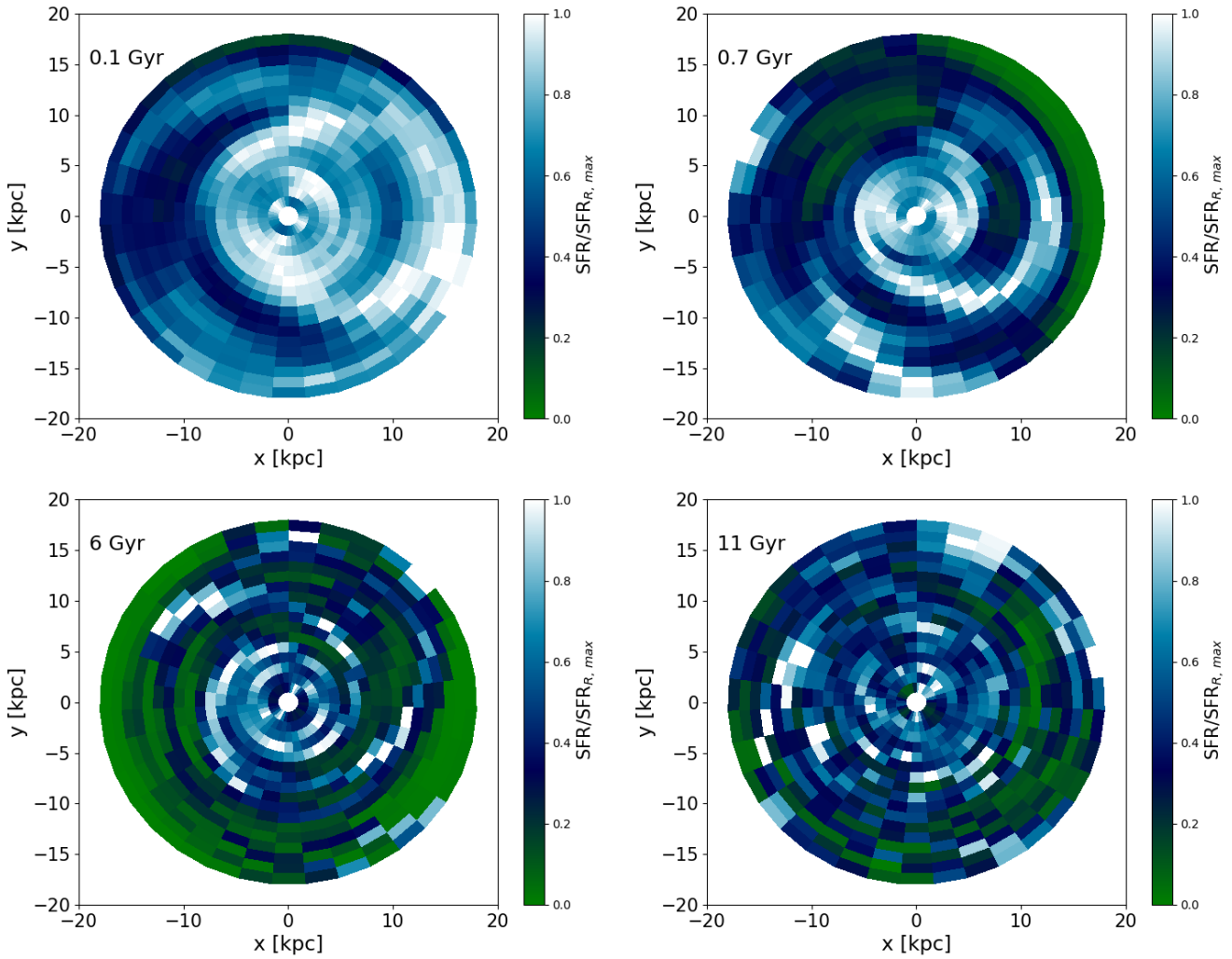


**Fig. 3.** The galactic disc SFR normalized to the maximum value  $\text{SFR}_{R, \max}$  of the annular region located at the Galactocentric distance  $R$ , i.e  $\text{SFR}(R, \phi)/\text{SFR}_{R, \max}$ , computed at 0.1, 0.7, 6, 11 Gyr after the start of disc formation, for the chemical evolution model in which we tested the effects of the density fluctuations by MCM13 model.

the presence of spiral arms and bar in a self consistent way. Our analytical spiral arms model is meant to break down the problem to understand the reason for the causes of azimuthal variations. Assuming that modes add linearly, we can approximate a realistic galactic disk by adding several spiral sets with different pattern speeds, as seen in observations (e.g., Meidt et al. 2009) and simulations (e.g., Masset & Tagger 1997, Quillen et al. 2011, Minchev et al. 2012a).

### 3. Results

In this section we apply our 2D model by using surface density fluctuations from the MCM13 chemo-dynamical model and from an analytical prescription.

#### 3.1. Density fluctuation from the MCM13 chemo-dynamical model

In this section we present our results based on the new 2D chemical evolution model including the density mass fluctuation extracted from the chemo-dynamical model by MCM13.

Fig. 2 shows the galactic disc SFR computed at 0.1, 0.7, 6, 11 Gyr after the start of disc formation, for the chemical evolution model in which we tested the effects of the density fluctuation by MCM13 in units of  $\text{M}_{\odot} \text{pc}^{-2} \text{Gyr}^{-1}$ . We notice that at early times (i.e the “1 Gyr” case reported in the upper left panel), the SFR is more concentrated in the inner Galactic regions, the SFR in the innermost regions decreases and the outer parts become more star forming active because of the “inside-out” prescription coupled with the inclusion of the density fluctuation. At the Galactic epoch of 1 Gyr after the start of disc formation, regions with the same Galactocentric distances have approximately the same SFR. Already after 0.7 Gyr of Galactic evolution, azimuthal star formation inhomogeneities are not negligible. Concerning the panel with the model results



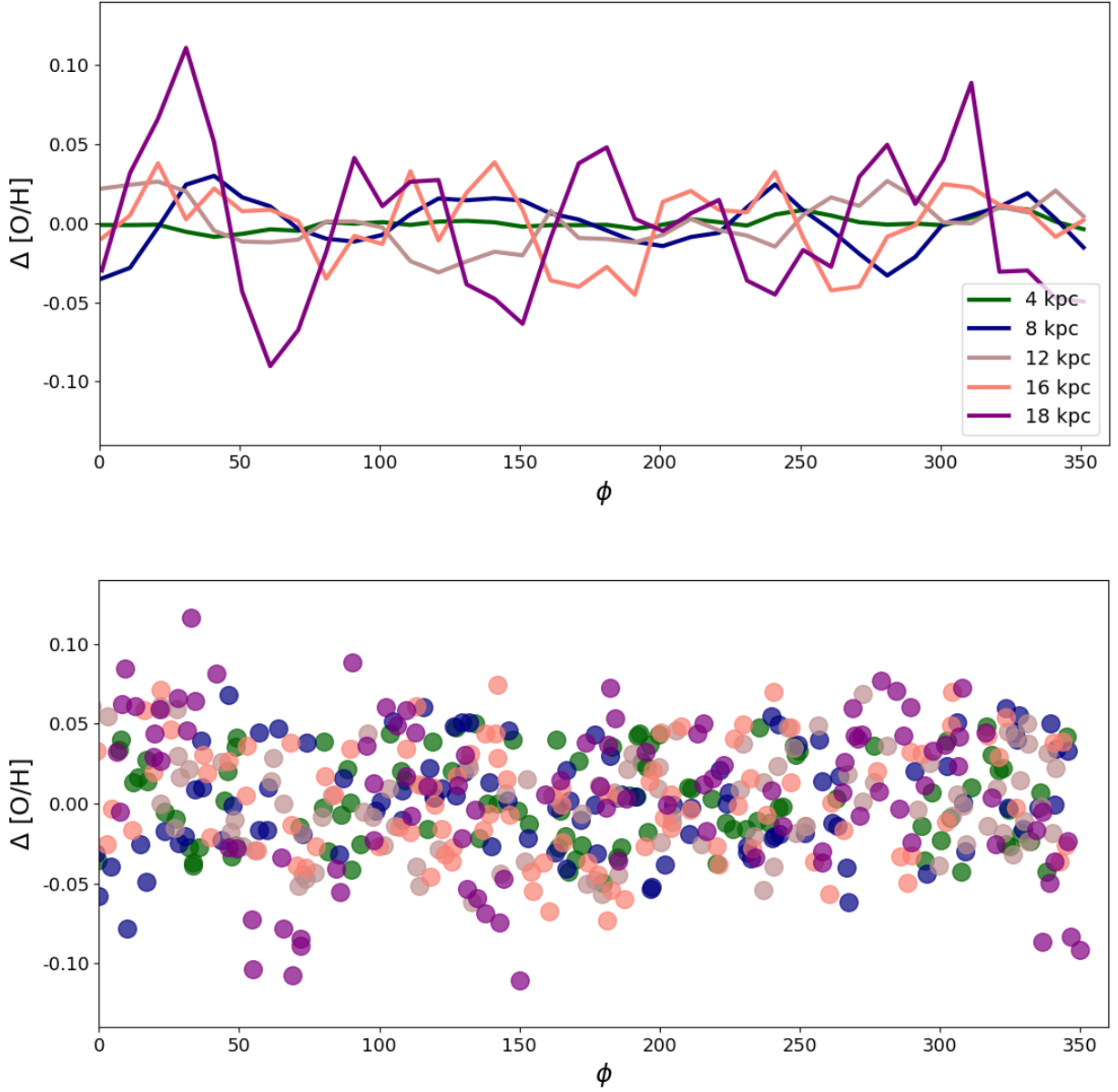


**Fig. 4.** Results for the chemical evolution model in which we consider the density fluctuation by the chemo-dynamical model by MCM13. *Upper Panel:* residuals of the ISM oxygen abundances as a function of Galactic azimuth computed with our chemical evolution model at 4, 8, 12, 16, and 18 kpc after subtracting the average radial gradient. *Lower Panel:* our mock observation to mimic Sánchez et al. (2015) results, in which we randomly plot residual ISM oxygen abundance predicted by our chemical evolution at 4, 8, 12, 16, and 18 kpc adding an uncertainty of  $5^\circ$  in the azimuthal component and taking into account [O/H] errors according to Sánchez et al. (2015); the color code is identical to line colors of the upper panel: innermost disc regions are associated with the green points, the outermost ones with the purple points.

at 6 Gyr, azimuthal inhomogeneities are evident, in particular at 8 kpc the ratio between the maximum and the minimum values assumed by the SFR is  $\text{SFR}_{\text{max}}/\text{SFR}_{\text{min}}=6.72$ .

In Fig. 2 the bar and spiral arms features do not show up clearly, especially in early times. This is caused by the adopted inside out prescription (eq. 4) which leads to huge differences between the SFRs computed in inner and outer regions. In Fig. 3, the galactic disc  $\text{SFR}(R, \phi)$  is normalized to the maximum value  $\text{SFR}_{R, \text{max}}$  of the annular region located at the

Galactocentric distance  $R$ , i.e.  $\text{SFR}(R, \phi)/\text{SFR}_{R, \text{max}}$ , computed at 0.1, 0.7, 6, 11 Gyr after the start of disc formation, respectively. Here, different features related to density perturbations originated by spiral arms and bar can be noted.

In Fig. 4 the main results related to the present day oxygen abundance azimuthal variation are presented. The top panel shows the azimuthal distribution of the residual of the oxygen abundances computed with our chemical evolution model at 4, 8, 12, 16, and 18 kpc after subtracting the average radial gra-

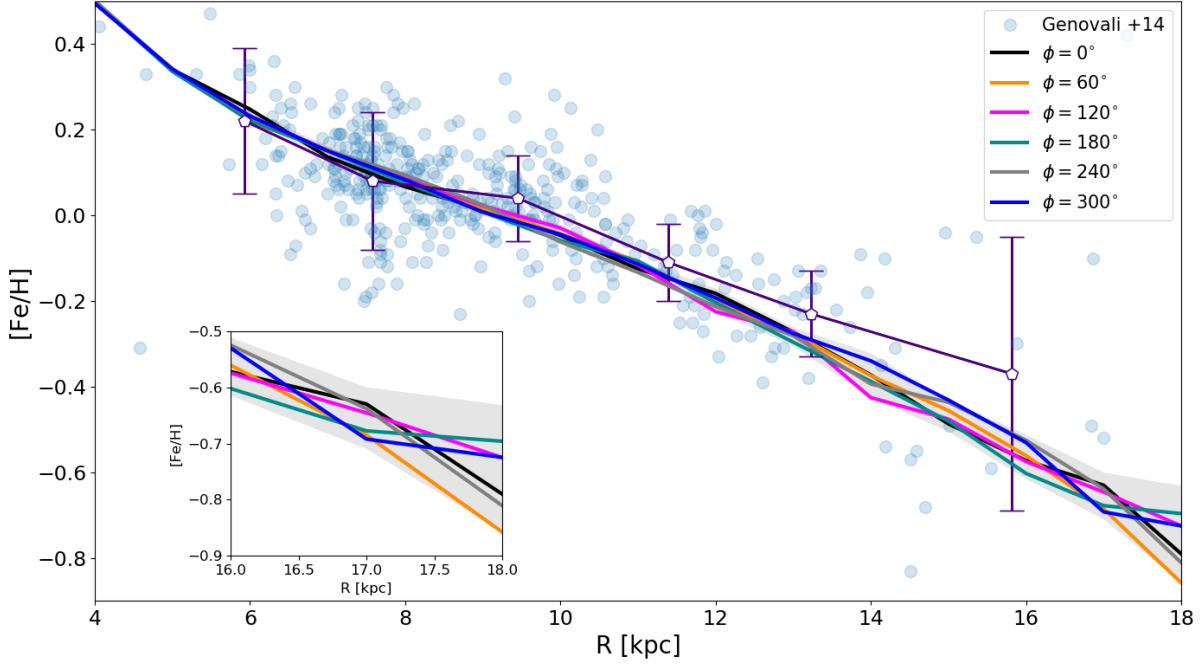


**Fig. 5.** Results for the chemical evolution model in which we consider the density fluctuation by the chemo-dynamical model by MCM13. The present day Fe abundance gradient computed at different azimuthal coordinates. The shaded grey area limits are related to the maximum and minimum iron abundance values at the different Galactocentric distances. Observational data (light blue circles) are the Cepheids collected by Genovali et al. (2014). With the empty pentagons we report the average abundance values and relative errors of Genovali et al. (2014) when divided into six radial bins. In the zoomed region are presented the model lines computed between 16 and 18 kpc.

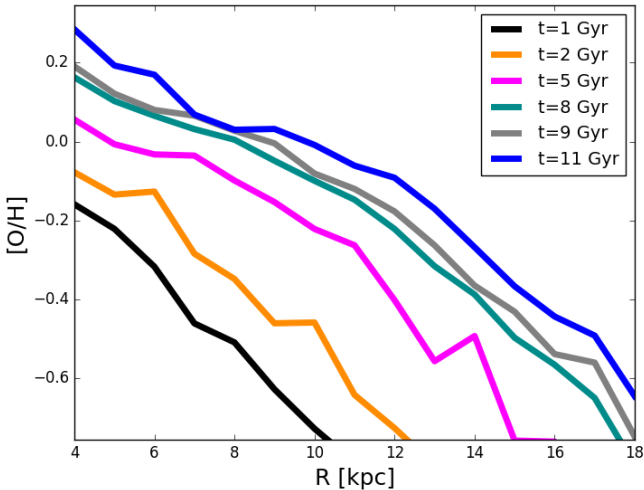


**Fig. 6.** Results for the chemical evolution model in which we consider the density fluctuation by the chemo-dynamical model by MCM13. Time evolution of the oxygen abundance gradient at  $\phi=0^\circ$ .

dient (i.e. the one obtained with the reference model without any density perturbation). Throughout this paper we adopt the photospheric values of Asplund et al. (2009) as our solar refer-

ence. We see that the behavior is in excellent agreement with the observations by Sánchez et al. (2015); indeed, data show that outer regions display larger azimuthal variations, and the amplitude of the residual variations are of the order of 0.1 dex (see Figure 7 by Sánchez et al. 2015). In our model the maximum variations are  $\sim 0.12$  dex for the chemical evolution models computed at 18 kpc. Our results appears to have a bit less scatter.

In the lower panel of Fig. 4 we present our “mock” observations. We draw oxygen abundances of different ISM regions at different Galactocentric distance at random azimuthal coordinates  $\phi$ . Hence, we add an error of  $\sigma_\phi=5^\circ$  to alleviate the fact that our model presents a resolution of  $10^\circ$  in the azimuthal component  $\phi$ . Moreover, the average observational uncertainty associated to the oxygen abundances of  $\sigma_{[O/H]} = 0.05$  dex provided by Sánchez et al. (2015) has been considered. We define the “new” oxygen abundance including these uncertainties as follows:

$$[O/H]_{new} = [O/H] + U([- \sigma_{[O/H]}, \sigma_{[O/H]}]), \quad (21)$$

where  $U$  is the random generator function. Similarly, we implement the uncertainty in the azimuthal component through the following relation:

$$\phi_{new} = \phi + U([- \sigma_\phi, \sigma_\phi]). \quad (22)$$

Here, it is clearly visible the similarity between the Sánchez et al. (2015) observations and our results. To summarize, the



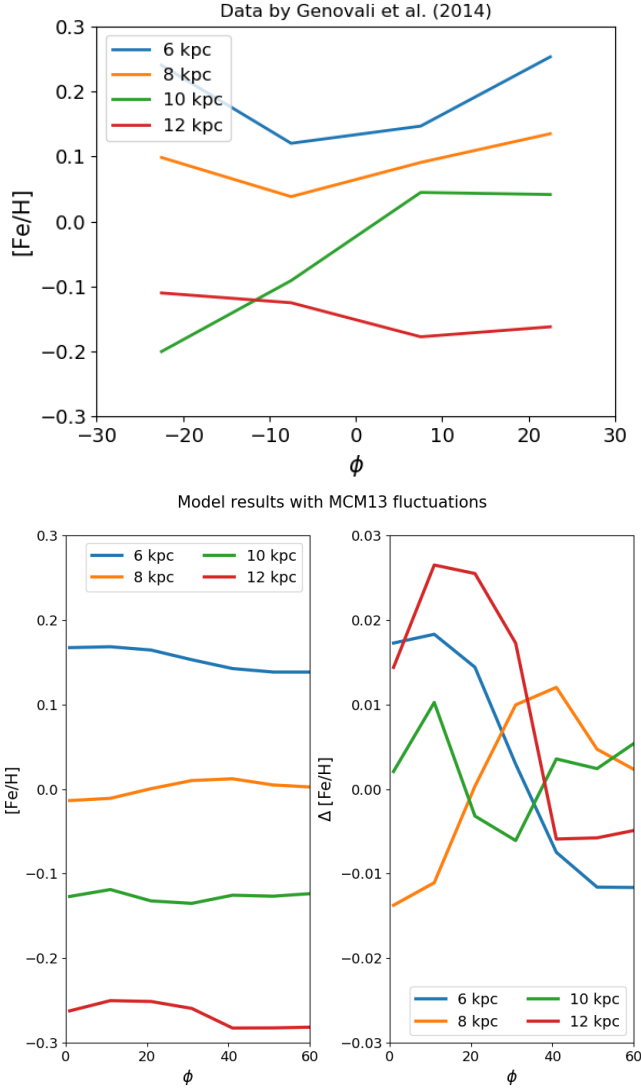


**Fig. 7.** *Upper Panel:* We present the average Fe abundances of Galactic Cepheids presented by Genovali et al. (2014) in bin of  $15^\circ$  for the azimuthal coordinate  $\phi$  at different Galactocentric distances. *Lower left Panel:* Fe abundances as functions of the azimuthal coordinates computed at 6, 8, 10, 12 kpc predicted by the chemical evolution model in which we implemented the density fluctuation by the MCM13 model. *Lower right Panel:* residual of the Fe abundances predicted by our model computed after subtracting the average radial gradient.

inclusions of density perturbations taken from a self-consistent dynamical model at different Galactic times, leads to significant variations in chemical abundances in the outer Galactic regions.

In Fig. 5 we show results for the present day abundance gradient (after 11 Gyr of evolution) for iron computed for six azimuthal slices (as indicated) of width  $10^\circ$  at different azimuthal coordinates. In the same plot is indicated with a shaded grey area the maximum spread in the abundance ratio  $[\text{Fe}/\text{H}]$  obtained by the azimuthal coordinates we considered ( $0^\circ$ ,  $60^\circ$ ,  $120^\circ$ ,  $180^\circ$ ,  $240^\circ$ , and  $300^\circ$ ). As a consequence of the results

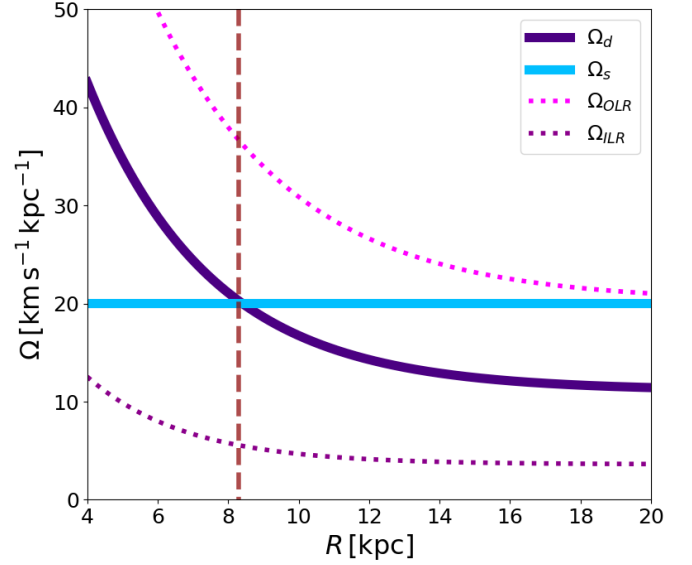


**Fig. 8.** Spiral pattern speed  $\Omega_s$  and disk angular velocity  $\Omega_d$  computed by Roca-Fàbrega et al. (2014) are indicated with light blue and violet lines, respectively. With the vertical long dashed red line we show the position of the corotation radius located at the Galactocentric distance  $R = 8.31 \text{ kpc}$ . Outer and Inner Lindblad resonances extracted by Roca-Fàbrega et al. (2014) simulation are also drawn with dotted magenta and dotted purple lines, respectively.

presented above, the shaded area is larger towards external regions. We also overplot the data from Genovali et al. (2014) in order to compare to our model predictions. We notice that the predicted gradient is slightly steeper than the observed one in the external Galactic regions. However, we notice that the model lines pass within in the data standard deviation computed dividing the data by Genovali et al. (2014) in six radial bins.

In Fig. 6 we tested the effects of chemo-dynamical fluctuations on the time evolution of the oxygen abundance gradient at a fixed azimuth ( $\phi=0^\circ$ ). In agreement with Minchev et al. (2018) the abundance gradient flattens in time, because of the chemical evolution model assumptions. As shown by Spitoni et al. (2015) and Grisoni et al. (2018), the inclusion of radial gas flows can in lead to even steeper gradients in time during the whole Galactic history.

In Fig. 7 we compare the average iron abundance azimuthal variation in bins of  $\phi=15^\circ$  presented by Genovali et al. (2014) computed at 6, 8, 10, and 12 kpc, respectively with our 2D chemical evolution model, resulting from the MCM13 density variations. We see that the observed azimuthal variations are for limited Galactocentric distances (6-12 kpc) and with a narrow range of azimuthal coordinates. Although it is evident that the observed amplitude of azimuthal variations are larger than the ones predicted by our models, more precise Galactic Cepheid data are required to make firm conclusions.

Moreover, other dynamical processes that we have not considered in this work had maybe played important roles in the evolution and in the building up of the Galactic gradients and

**Table 1.** Different spiral arm models tested with our 2D chemical evolution model for the disc changing the number of spiral arms  $m$  (second column), the pitch angle  $\alpha$  (third column), and finally the spiral pattern speed  $\Omega_s$  is indicated in the last column.

Models	$m$	$\alpha$	$\Omega_s$ [km s <sup>-1</sup> kpc <sup>-1</sup> ]
S2A	2	15°	20
S2B	2	15°	17.5
S2C	2	15°	15
S2D	2	15°	13.75
S2E	2	15°	12.5
S2F	2	15°	25
S2G	2	7°	20
S2H	2	30°	20
S1A	1	15°	20
S1B	1	15°	17.5
S1C	1	15°	15
S1D	1	15°	13.75
S1E	1	15°	12.5
S1F	1	15°	25

their azimuthal variations - radial migration processes can already introduce some variations in about a Gyr (Quillen et al. 2018).

### 3.2. Density fluctuations from an analytical spiral arm formulation

In this Section we discuss the results of chemical evolution models with only analytical prescriptions for spiral arm density perturbations without including any density fluctuations from chemo-dynamical models. The primary purpose here is to test the effect of regular perturbations (i.e. spiral arms evolution described by an analytical formulation) on the chemical evolution of a Milky Way like galaxy. We underline that the results showed in the previous Section reflect more closely the complex behavior of the Milky Way. However, we are also interested to explore different spiral arm configurations which could characterize external galactic systems by varying the free parameters of the analytical expression of the spiral arms. In particular, we will show the effects on the azimuthal variations of abundance gradients for oxygen by varying:

- i) the multiplicity  $m$  of spiral arms;
- ii) the spiral pattern speed,  $\Omega_s$ ;
- iii) the pitch angle  $\alpha$ .

For all model results that will be presented we assume the following Cox & Gomez (2002) prescriptions: the radial scale length of the drop-off in density amplitude of the arms fixed at the value of  $R_S = 7$  kpc, the pitch angle is assumed constant at  $\alpha = 15^\circ$ , and the surface arm density  $\Sigma_0$  is  $20 \text{ M}_\odot \text{ pc}^{-2}$  at the fiducial radius  $R_0 = 8$  kpc; finally we assume  $\phi_p(R_0) = 0$ .

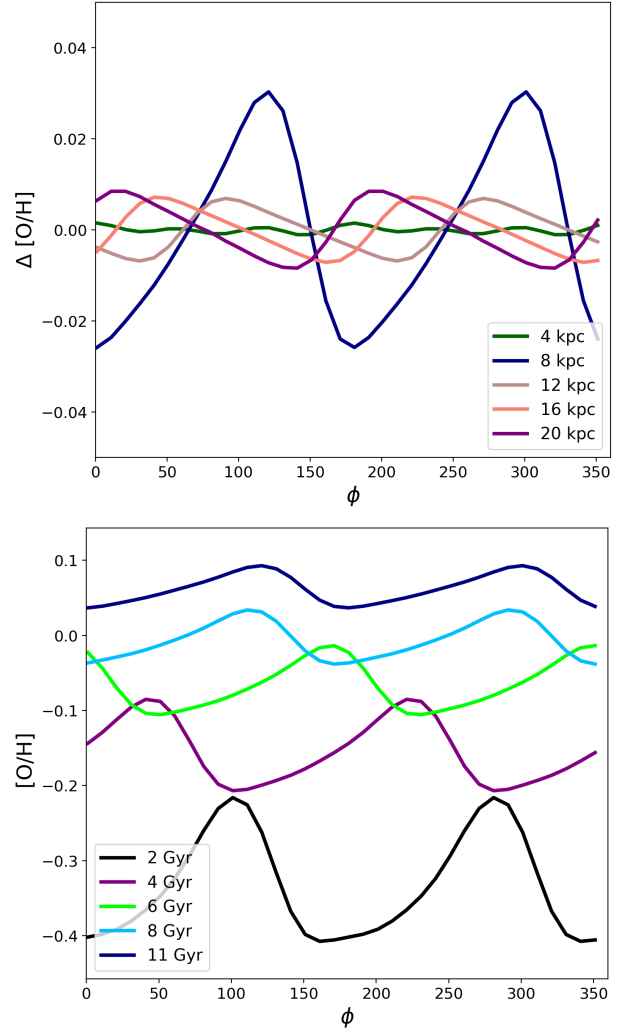


**Fig. 9.** Results for the chemical evolution model in which we consider the density fluctuation associated with the analytical spiral arm formulation. *Upper Panel:* The azimuthal distribution of the residual of the oxygen abundances computed with our chemical evolution model at 4, 8, 12, 16, and 20 kpc (after subtracting the average radial gradient for a model with  $R_S=7$ ,  $R_D=3.5$ ,  $\Sigma_0=20$ ,  $\nu=1.1$ ,  $\Omega_s=20 \text{ km s}^{-1} \text{ kpc}^{-1}$ , and  $m=2$  spiral arm (model S2A in Table 1). *Lower Panel:* the time evolution of the [O/H] abundance as a function of the azimuthal coordinate computed at 8 kpc.

The disk rotational velocity  $\Omega_d(R)$  has been extracted from the simulation by Roca-Fàbrega et al. (2014) (see their left panel of Figure 1). The exponential fit of  $\Omega_d(R)$  variations as a function of the Galactocentric distance  $R$  (expressed in kpc) is:

$$\Omega_d(R) = 98.93 e^{-0.29R} + 11.11 \text{ [km s}^{-1} \text{ kpc}^{-1}]. \quad (23)$$

We start by adopting the constant pattern angular velocity  $\Omega_s = 20 \text{ km s}^{-1} \text{ kpc}^{-1}$  consistent with the Roca-Fàbrega et al. (2014) model. Similar value was first estimated from moving groups in the U-V plane by Quillen & Minchev (2005,  $18.1 \pm 0.8 \text{ km s}^{-1} \text{ kpc}^{-1}$ ) and a summary of derived values for the Milky Way can be found in Bland-Hawthorn & Gerhard (2016). In Fig. 8

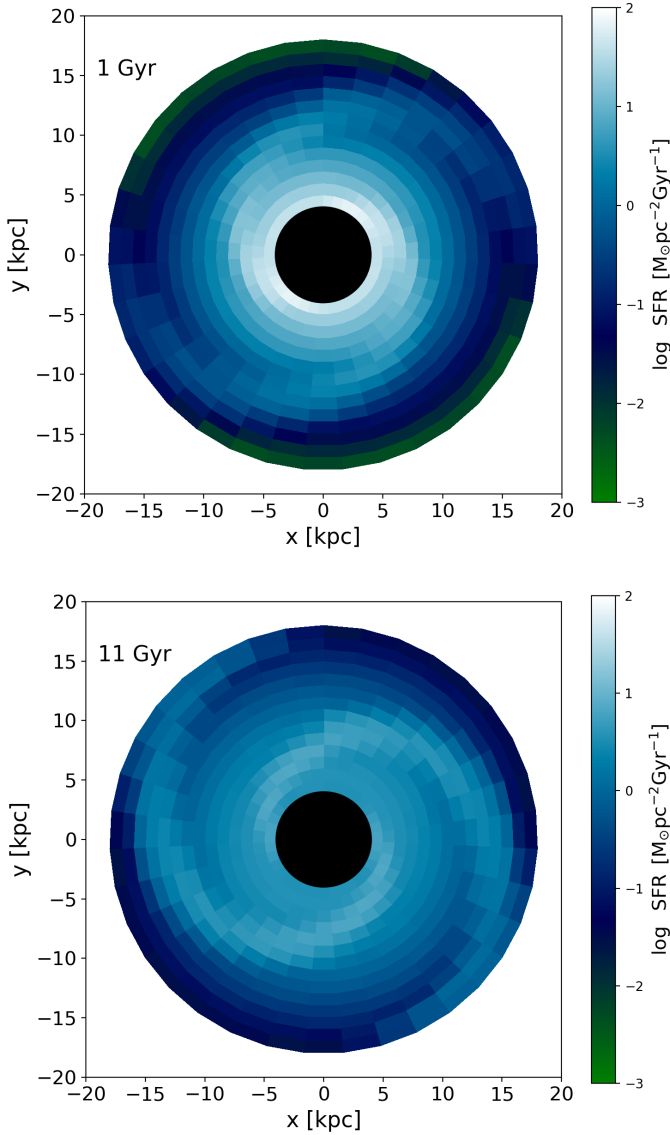


**Fig. 10.** *Upper Panel:* Galactic disc SFR resulting from model S2A after 1 Gyr of evolution (see Table 1 and text for model details). The color code indicates the SFR in units of  $M_{\odot} \text{pc}^{-2} \text{Gyr}^{-1}$ . *Lower Panel:* same but computed at 11 Gyr.

we show the  $\Omega_s$  and  $\Omega_d(R)$  quantities as well as the Outer and Inner Lindblad resonances as a function of the Galactocentric distance, the corotation radius is located at 8.31 kpc.

### 3.2.1. Results with a single analytical spiral pattern

We begin our analysis discussing the results obtained with model S2A (see Table 1), which has a pattern speed of  $\Omega_s = 20 \text{ km s}^{-1} \text{kpc}^{-1}$ , placing the corotation resonance at the solar radius.

The upper panel of Fig. 9 shows the the oxygen abundance residual azimuthal variations after 11 Gyr of disc evolution for different Galactocentric distances. The average radial gradient is subtracted. As expected, larger abundance azimuthal variations are found near the corotation radius. In this region the

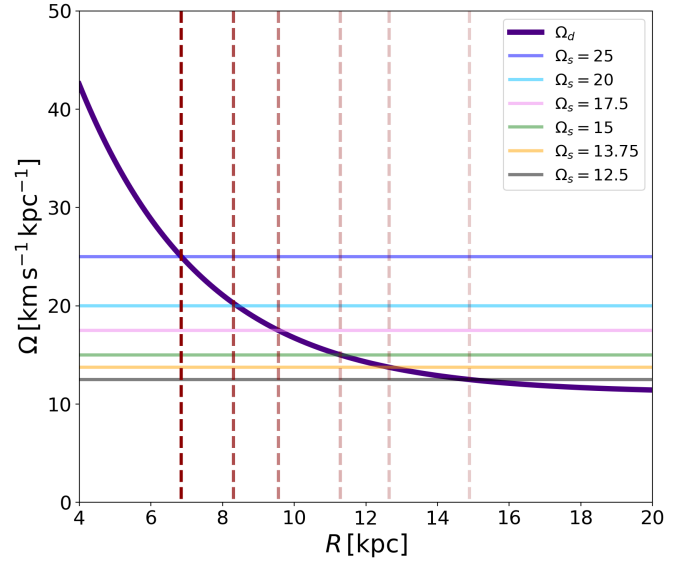


**Fig. 11.** Disk angular velocity  $\Omega_d$  computed by Roca-Fàbrega et al. (2014) is indicated with light blue and violet lines. With different horizontal solid lines are indicated the spiral pattern speed  $\Omega_s$  adopted in our models (see text and Table 1 for model details). The vertical long dashed lines show the positions of the corotation radii assuming different  $\Omega_s$  values.

chemical enrichment should be more efficient due to the lack of the relative gas-spiral motions. Higher SFR at the corotation radius caused by locally higher gas overdensity lasts for a longer time, therefore more massive stars can be created and more metals can be ejected into the local ISM under the spiral arm passage.

At 8 kpc we have  $\Delta[\text{O}/\text{H}] \approx 0.05$  dex. For other Galactocentric distances, away from the corotation, variations are much smaller. In the lower panel of Fig. 9 we present the temporal evolution of the oxygen abundance azimuthal variations for the model S2A as a function of the azimuthal coordinate  $\phi$  computed at 8 kpc. As expected, larger inhomogeneities are present at early times, decreasing in time.

As discussed in Section 2.2, we assume that during the Galactic evolution the ratio between the amplitude of the spiral density perturbation and the total surface density computed at the same radius  $R$ , remains constant in time. However, this analytical approach is not capable to put constraints on the temporal evolution of pattern speed.

Galactic chemical evolution is an integral process in time. The stronger spiral structure induced azimuthal variations at early times are, therefore, washed out by phase mixing.

Fig. 10 depicts the SFR after 1 Gyr of evolution (upper panel) and at the present time (lower panel) on the galactic plane computed with the model S2A. Here, it is evident the way in which the spiral arm density perturbation affects and modulates SFR computed at the present time in unit of  $M_{\odot} \text{pc}^{-2} \text{Gyr}^{-1}$ . The shape of the two spiral arm over-densities is clearly visible in the SFR. This is in contrast to our results using the MCM13 density fluctuations (see Fig. 2), where multiple spiral density waves were present. Moreover, we can appreciate the

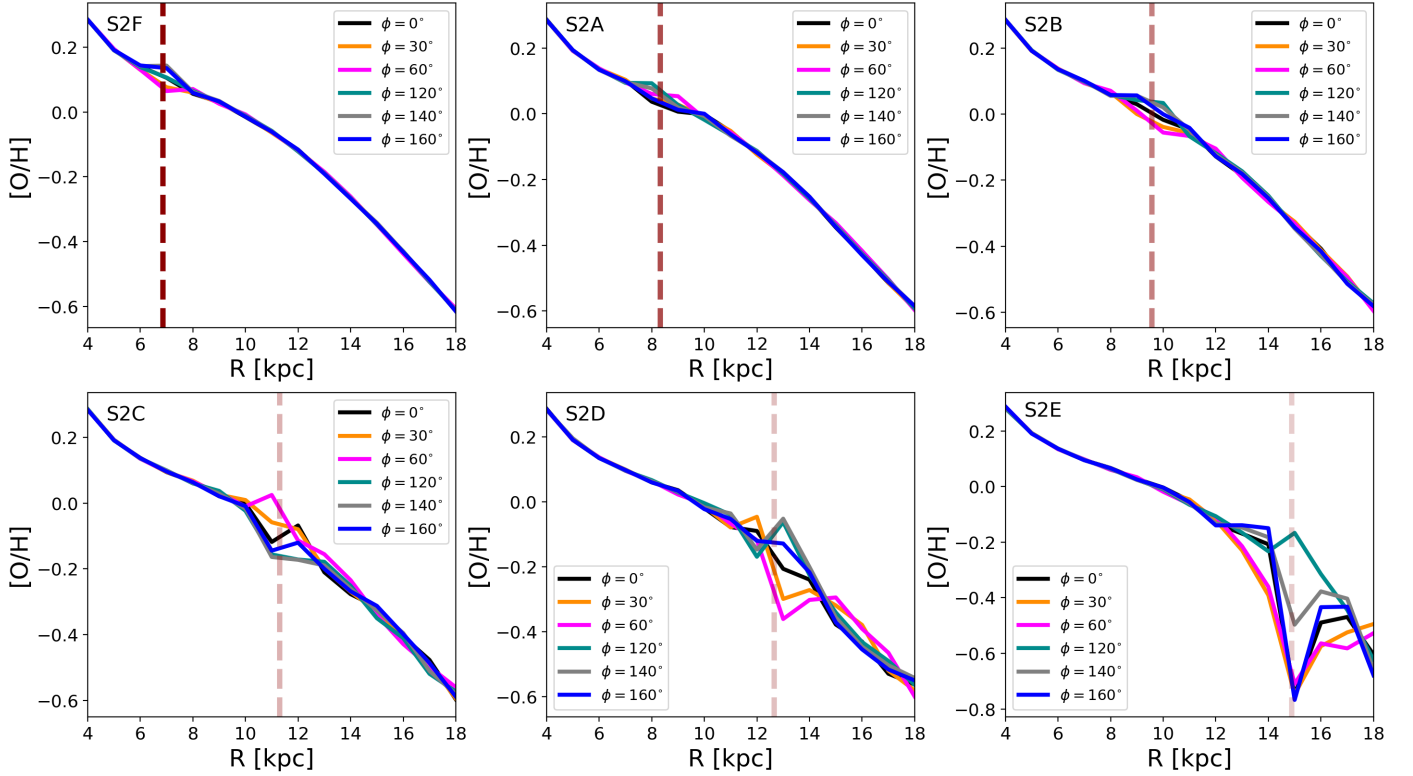


**Fig. 12.** The present day oxygen abundance gradients for different azimuths, predicted by chemical models with spiral multiplicity  $m = 2$  and different spiral pattern speed  $\Omega_s$  (see Table 1 for model details). In each panel the dashed vertical line indicates the location of the corotation radius. It is clear that allowing for multiple spiral patterns propagating through the disk at the same time will affect the entire disk, similarly to the case of the MCM13 model.

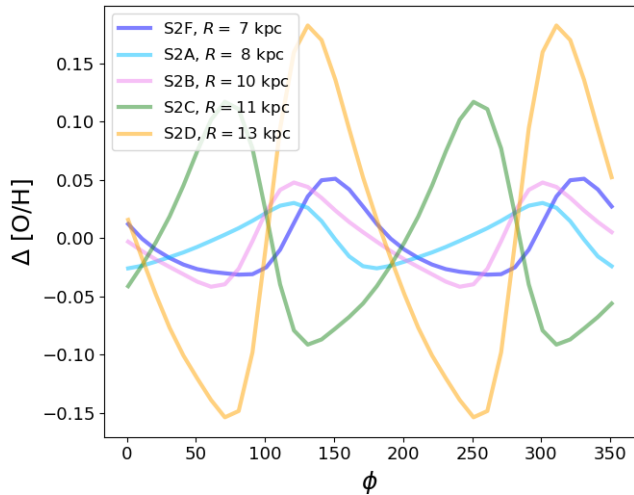


**Fig. 13.** Present day residual azimuthal variations in oxygen abundance for the corotation regions (as indicated) of the different pattern speeds shown in Fig. 12. An increase in the effect is found as the corotation shifts to larger radius, i.e., for slower spiral patterns. Such a set of spirals with progressively slower patterns speeds as radius increases, can be a realistic representation of a galactic disk.

inside-out disk formation: at later times the external regions become star formation active.

### 3.2.2. The effect of different pattern speeds

In this Section we vary the spiral pattern speed, which has the effect of shifting the corotation resonance in radius. We argue that a combination of multiple spiral modes with different pattern speeds can be a realistic representation of a galactic disk. The horizontal and vertical lines in Fig. 11 show the different pattern speeds and corresponding corotation radii, respectively, used in this Section: it is clear that smaller  $\Omega_s$  values lead to a more external corotation radius.

In Fig. 12 we show the oxygen abundance gradients computed at different azimuths after 11 Gyr of disk evolution for models with spiral multiplicity  $m = 2$  and different spiral pattern speed  $\Omega_s$  (see Table 1 for model details).

We notice that the more the corotation radius is shifted towards the external Galactic regions the more the oxygen azimuthal abundance variations are amplified near the corotation radius. This result is reasonable in the light of our previous findings presented above with our model assuming chemodynamical fluctuations by MCM13. We recall that larger variations in the chemical abundance of outer galactic regions have been found by observations in external galaxies (Sánchez et al. 2015).

In Fig. 13 we show the present day azimuthal residual of the oxygen abundances after subtracting the average radial gradient computed for the Galactic annular regions which include the relative corotation radius for the following models with

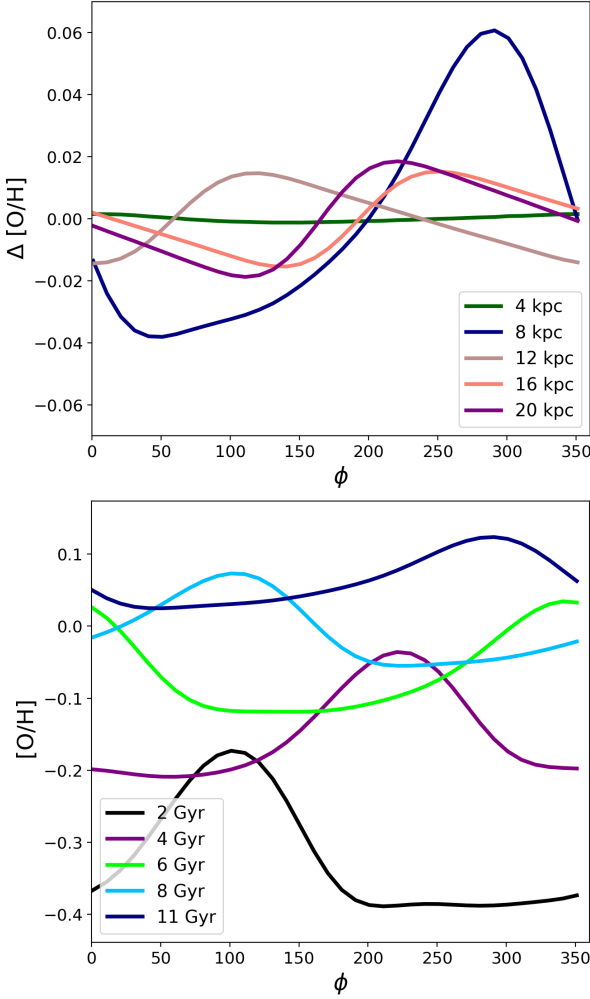


**Fig. 14.** As in Fig. 9 but for model S1A, with with multiplicity  $m=1$  of spiral arms.

$m = 2$  multiplicity: S2A, S2B, S2C, S2D, S2F (see Table 1 for other parameter details). The model S2D computed at  $R = 13$  kpc has  $\Delta[O/H] \approx 0.32$  dex. Already in regions not so far from the solar neighbour, the variations are important, i.e., model S2C whose corotation resides in the annular region centered at  $R = 11$  kpc, presents an oxygen abundance variation of  $\Delta[O/H]$  is  $\approx 0.20$  dex.

As discussed in Section 2.3, it is well accepted that multiple patterns can be present in galactic disks (e.g., Meidt et al. 2009) including our own Milky Way (Minchev & Quillen 2006, Quillen et al. 2011), with slower patterns shifted to outer radii. This will have the effect of placing the corotation regions very similarly to what Fig. 13 presents and having corotating arms at all radii as found by Grand et al. (2012), Hunt et al. (2019). Therefore, the increasing scatter in abundance with galactic radius can be explained as the effect of multiple patterns propagating at the same time. Note that radial migration will introduce additional scatter, that can in principle be accounted for.

### 3.2.3. Results with an $m=1$ spiral pattern

We want to test whether the intensity of the amplitude of the azimuthal chemical abundance variations is dependant on the number  $m$  of spiral arms. In Table 1 we label as model S1A a model identical to the model S2A but with an  $m=1$  spiral structure, i.e., having only one spiral arm. Such a mode arises naturally from the coupling of  $m=2$  and  $m=3$  modes as found by Quillen et al. (2011) and Minchev et al. (2012a) using pure N-body and SPH simulations, and is seen in external galaxies (Zaritsky & Rix 1997).

In the upper panel of Fig. 14 we notice that the abundance variations are larger than the ones obtained with the same model but  $m=2$  (upper panel of Fig. 9): a fluctuation of about  $\Delta[O/H]=0.1$  dex is seen at the corotation radius ( $\sim 8$  kpc).

In the same Figure is presented the time evolution of azimuthal abundance inhomogeneities for oxygen computed at 8 kpc with the model S1A at 2, 4, 6, 8, and 11 Gyr.

In Fig. 15 we have the oxygen abundance gradients computed at different azimuths after 11 Gyr of disk evolution for models with spiral multiplicity  $m = 1$  and the same spiral pattern speeds  $\Omega_s$  as in Fig. 12 (see Table 1 for model details). We notice that around the corotation radii the azimuthal abundance variations are generally more evident for models with one spiral arm compared to ones with spiral multiplicity  $m = 2$ .

In Fig. 16 we show the present day azimuthal residual of the oxygen abundances after subtracting the average radial gradient computed in annular regions which contain the corotation radii for models with  $m = 1$  multiplicity: S1A, S1B, S1C, S1D, S1F (see Table 1 for other parameter details). For the model S1D at the Galactic distance of 13 kpc we have  $\Delta[O/H] \approx 0.40$  dex, which is about  $\approx 25\%$  larger than the S2D case. As found for the model with  $m = 2$ , the oxygen abundance variations become important in regions not so far from the solar vicinity, i.e., model S1C whose corotation resides at  $R = 11$  kpc,  $\Delta[O/H] \approx 0.23$  dex.

### 3.2.4. Results for different pitch angles

In this Section we consider different pitch angles  $\alpha$  for the spiral arms in our Milky Way galaxy.

Recent work by Quillen et al. (2018) and Laporte et al. (2018) suggest that tightly wound spiral structure should be considered, based on modeling of phase-space structure found in the second Gaia data release (Gaia collaboration et al. 2018).

A smaller pitch angle gives rise to more tightly wound spiral structure. The upper panel of Fig. 17 depicts the present time SFR computed with a pitch angle  $\alpha = 7^\circ$  (model S2G in Table 1), whereas the lower panel shows the case of  $\alpha = 30^\circ$  (model S2H in Table 1). For both panels the other model parameters as the same as model S2A. The spiral pattern is clearly visible in the SFR, and for the model S2G a tighter wound spiral structure is present.

In Fig 18 we compare the azimuthal variations for models S2G and S2H. We see that the chemical variations are identical at the corotation radius and simply azimuthally shifted for other Galactocentric distances.



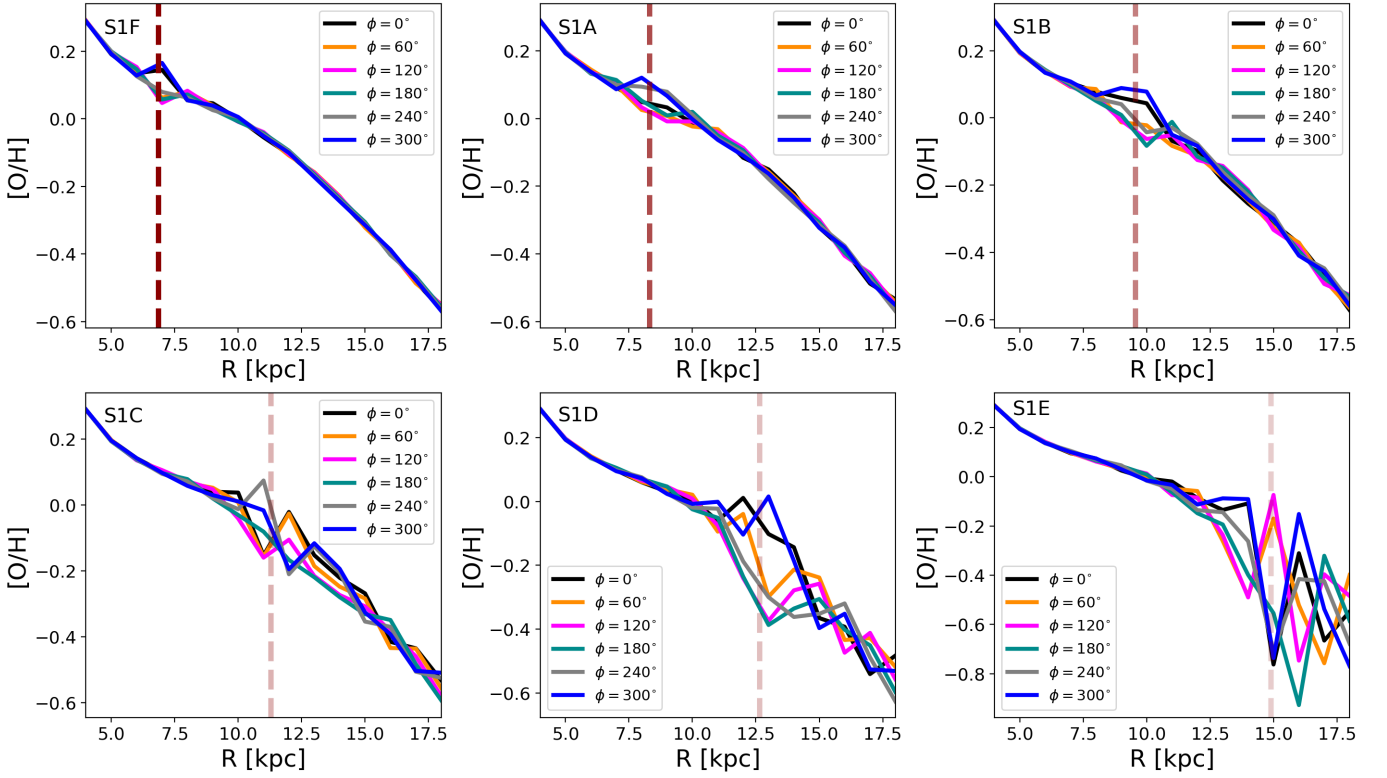


**Fig. 15.** As Fig. 12, but for an  $m=1$  spiral.

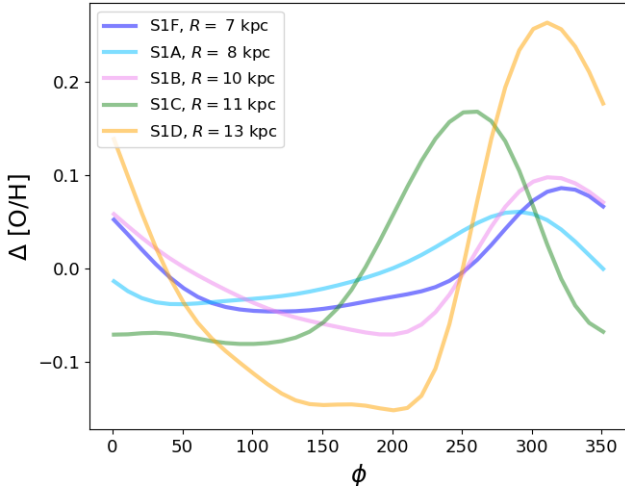


**Fig. 16.** As in Fig. 13 but for models with  $m = 1$  multiplicity (see Table 1).

#### 4. Conclusions

In this paper we presented a new 2D chemical evolution model, able to trace azimuthal variations in the galactic disc density. We applied this model to (i) the density fluctuations arising in a disc formation simulation by Martig et al. (2012), used for the MCM13 Milky Way chemo-dynamical model, and (ii) the density perturbations originating from an analytical spiral arm formulation.

The main conclusions for density perturbation from Milky Way chemo-dynamical model by MCM13 can be summarized as follows:

- We found that the density fluctuations produce significant oxygen azimuthal variations in the abundance gradients of the order of 0.1 dex.
- The azimuthal variations are more evident in the external galactic regions, in agreement with the recent observations of the galaxy NGC 6754, using MUSE data (Sánchez et al. 2015).

In an effort to understand the above findings, we constructed simple analytical spiral arm models, for which we varied the pattern speed, multiplicity and pitch angle with the following main findings:

- The larger fluctuations in the azimuthal abundance gradients are found near the corotation radius, where the relative velocity with respect to the disk is close to zero.
- Larger azimuthal variations are found at corotation radii shifted to larger radii, i.e., slower pattern speeds.
- The variation is more enhanced for the model with only one spiral arm, which is expected to result from the combination of an  $m=2$  and  $m=3$  spiral structure.
- We found that the more significant azimuthal abundance variations seen at early times in presence of a regular, periodic perturbation tend to quench at later times. This is expected, as galactic chemical evolution is cumulative process and phase-mixing and radial migration tends to wipe structure with time.



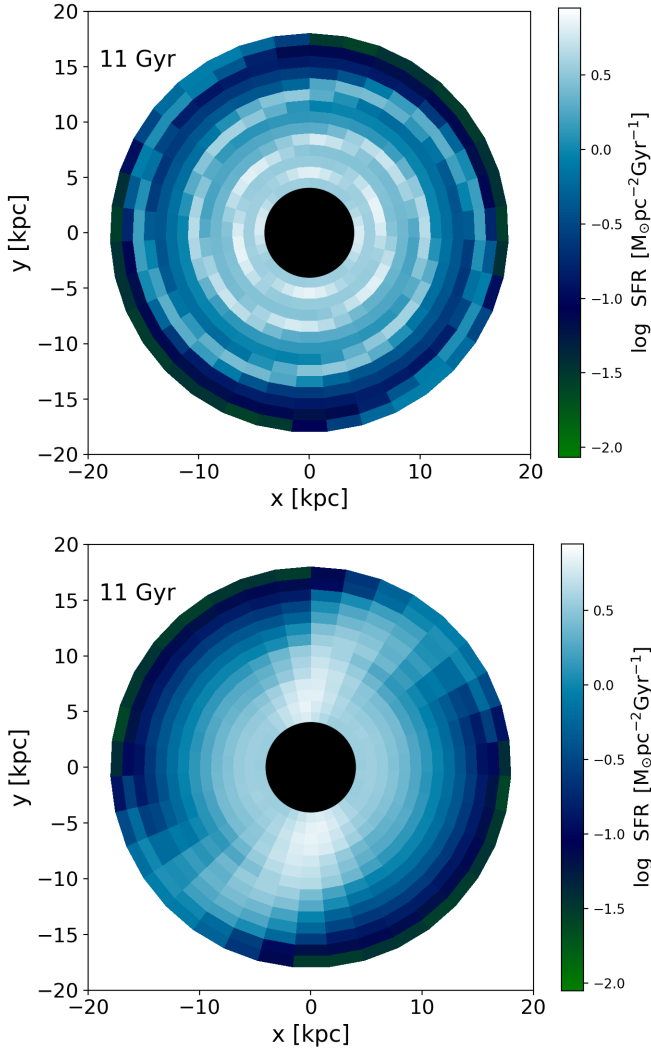


**Fig. 17.** *Upper Panel:* The Galactic disc SFR related to the model S2G computed after 11 Gyr of Galactic evolution (see Table 1 and text for model details) with a pitch angle  $\alpha = 7^\circ$ . The color code indicates the SFR in units of  $M_\odot \text{ pc}^{-2} \text{ Gyr}^{-1}$ . *Lower Panel:* as the upper panel but for the model S2H where the pitch angle  $\alpha$  is  $30^\circ$ .

Combining the effect of corotation radii by assuming the simultaneous propagation of multiple spiral modes through galactic disks, we can obtain a realistic picture of azimuthal variations induced at stellar birth found in self-consistent models, such as the MCM13. Material spiral arms propagating near the corotation at all galactic radii have been described by a number of recent numerical work with different interpretations (see Grand et al. 2012, Comparetta & Quillen 2012, Hunt et al. 2019).

In future work we will improve the new 2D chemical evolution model introduced here by taking into account stellar radial migration of long-lived stars and the pollution to the ISM abundance introduced by them at radii and azimuths different than their birth places. We will also use this model to update the Galactic habitable zone results presented by Spitoni et al. (2014, 2017) and study the effect of spiral structure and the Galactic bar.

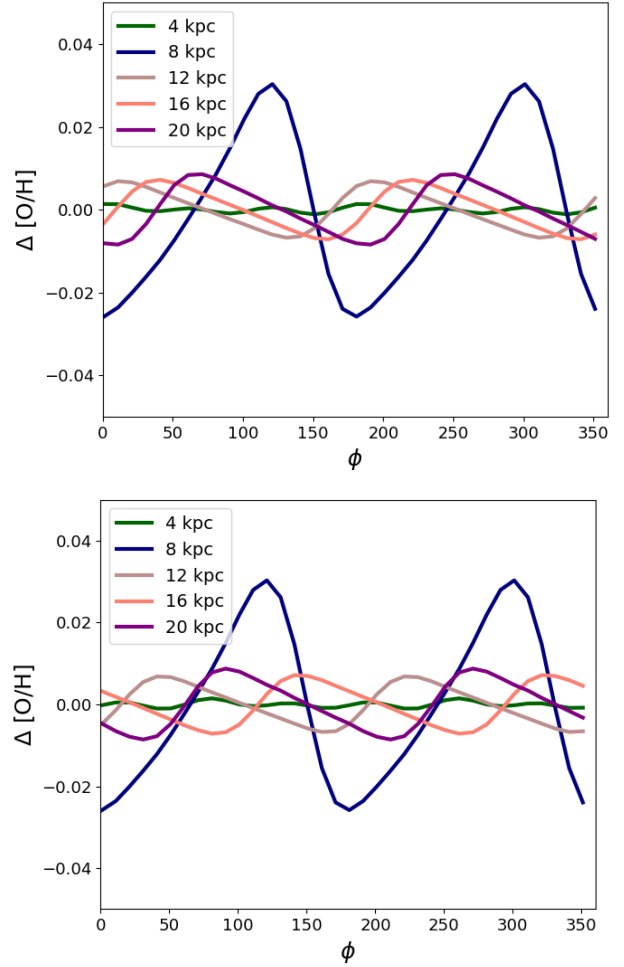


**Fig. 18.** Effects of different pitch angles  $\alpha$  on the azimuthal distribution of the residual of the oxygen abundances computed with our chemical evolution model at 4, 8, 12, 16, and 20 kpc. In the upper panel the pitch angle is set at the value of  $7^\circ$  (SE model in Table 1), while in the lower panel  $\alpha = 30^\circ$  (SF model in Table 1).

## Acknowledgement

We thank the anonymous referee for various suggestions that improved the paper. E. Spitoni and V. Silva Aguirre acknowledge support from the Independent Research Fund Denmark (Research grant 7027-00096B). V. Silva Aguirre acknowledges support from VILLUM FONDEN (Research Grant 10118). G. Cescutti acknowledges financial support from the European Union Horizon 2020 research and innovation programme under the Marie Skłodowska-Curie grant agreement No. 664931. This work has been partially supported by the EU COST Action CA16117 (ChETEC). I. Minchev acknowledges support by the Deutsche Forschungsgemeinschaft under the grant MI 2009/1-1. F. Matteucci acknowledges research funds from the University of Trieste (FRA2016).

## References

- Asplund, M., Grevesse, N., Sauval, A. J., & Scott, P. 2009, *ARA&A*, 47, 481
- Balser, D. S., Wenger, T. V., Anderson, L. D., Bania, T. M., 2015, *ApJ*, 806, 199
- Bertin, G., Lin, C. C., Lowe, S. A., Thurstans, R. P., 1989, *ApJ*, 338, 78
- Bland-Hawthorn, J., & Gerhard, O. 2016, *ARAA*, 54, 529
- Cescutti, G., Chiappini, C., 2010, *A&A*, 515, A102
- Cescutti, G., François, P., Matteucci, F., Cayrel, R., Spite, M., 2006, *A&A*, 448, 557
- Cescutti, G., Matteucci, F., François, P., Chiappini, C., 2007, *A&A*, 462, 943
- Chiappini, C., Matteucci, F., Romano, D., 2001, *ApJ*, 554, 1044
- Comparetta, J., & Quillen, A. C., 2012, *arXiv:1207.5753*
- Cox, D. P., Gómez, G. C. 2002, *ApJS*, 142, 261
- Davies, B., Origlia, L., Kudritzki, R.-P., et al., 2009, *ApJ*, 696, 2014
- Dehnen, W., Binney, J., 1998, *MNRAS*, 294, 429
- Dib, S., Piau, L., Mohanty, S., & Braine, J. 2011, *MNRAS*, 415, 3439
- Elmegreen, B. G., Elmegreen, D. M., & Montenegro, L. 1992, *ApJs*, 79, 37
- Faure, C., Siebert, A., Famaey, B., 2014, *MNRAS*, 440, 2564
- François P., Matteucci F., Cayrel R., et al. 2004, *A&A*, 421, 613
- Gaia Collaboration, Katz, D., Antoja, T., et al. 2018, *A&A*, 616, A11
- Genovali, K., Lemasle, B., Bono, G., et al. 2014, *A&A*, 566, A37
- Genovali, K., Lemasle, B., da Silva, R., et al., 2015, *A&A*, 580, A17
- Gerhard, O., 2011, *Memorie della Societa Astronomica Italiana Supplementi*, 18, 185
- Grand, R. J. J., Kawata, D., Cropper, M. 2012, *MNRAS*, 426, 167
- Grand, R. J. J., Kawata, D., Cropper, M. 2014, *MNRAS*, 439, 623
- Grand, R. J. J., Springel, V., Kawata, D., et al., 2016, *MNRAS*, 460, L94
- Grisoni, V., Spitoni, E., Matteucci, F., 2018, *MNRAS*, 481, 2570
- Ho, I.-T., Seibert, M., Meidt, S. E., et al., 2017, *ApJ*, 846, 39
- Hunt, J. A. S., Bub, M. W., Bovy, J., et al., 2019, *arXiv:1904.10968*
- Iwamoto, K., Brachwitz, F., Nomoto, K., et al. 1999, *ApJ Suppl. Ser.*, 125, 439
- Laporte, C. F. P., Minchev, I., Johnston, K. V., & Gómez, F. A. 2018, *arXiv:1808.00451*
- Li, Y., Bresolin, F., Kennicutt, R. C., Jr., 2013, *ApJ*, 766, 17
- Lin, C. C., & Shu, F. H., 1966, *Proceedings of the National Academy of Science*, 55, 229
- Kennicutt, R. C., Jr. 1998, *ApJ*, 498, 541
- Khoperskov, S., Di Matteo, P., Haywood, M., Combes, F., 2018, *A&A*, 611, L2
- Martig, M., Bournaud, F., Croton, D. J., Dekel, A., Teyssier, R., 2012, *ApJ*, 756, 26
- Martig, M., Minchev, I., Ness, M., Fouesneau, M., & Rix, H.-W. 2016, *ApJ*, 831, 139
- Masset, F., & Tagger, M. 1997, *A&A*, 322, 442
- Matteucci, F., François, P., 1989, *MNRAS*, 239, 885
- Meidt, S. E., Rand, R. J., Merrifield, M. R. 2009, *ApJ*, 702, 277
- Meynet, G., Maeder, A., 2002, *A&A*, 390, 561
- Minchev, I., Anders, F., Recio-Blanco, A., et al., 2018, *MNRAS*, 481, 1645
- Minchev, I., Chiappini, C., & Martig, M. 2013, *A&A*, 558, A9
- Minchev, I., Chiappini, C., & Martig, M. 2014, *A&A*, 572, A92
- Minchev, I., Famaey, B., Quillen, A. C., et al. 2012a, *A&A*, 548, A126
- Minchev, I., Famaey, B., Quillen, A. C., et al. 2012b, *A&A*, 548, A127
- Minchev, I., Martig, M., Streich, D., et al., 2015, *ApJL*, 804, L9
- Mott, A., Spitoni E., Matteucci F., 2013, *MNRAS*, 435, 2918
- Pedicelli, S., Bono, G., Lemasle, B., et al., 2009, *A&A*, 504, 81
- Pettitt, A. R., Tasker, E. J., & Wadsley, J. W., 2016, *MNRAS*, 458, 3990
- Quillen, A. C., Dougherty, J., Bagley, M. B., Minchev, I., & Comparetta, J. 2011, *MNRAS*, 417, 762
- Quillen, A. C., Carrillo, I., Anders, F., et al. 2018, *MNRAS*, 480, 3132
- Quillen, A. C., & Minchev, I. 2005, *AJ*, 130, 576
- Ragan, S. E., Moore, T. J. T., Eden, D. J., et al., 2018, *MNRAS*, 479, 2361
- Renaud, F., Bournaud, F., Emsellem, E., et al. 2015, *MNRAS*, 454, 3299
- Rix, H.-W., & Zaritsky, D. 1995, *ApJ*, 447, 82
- Roberts, W. W., 1969, *ApJ*, 158, 123
- Roca-Fàbrega, S., Antoja, T., Figueras, F., et al., 2014, *MNRAS*, 440, 1950
- Romano D., Karakas A. I., Tosi M., Matteucci F., 2010, *A&A*, 522, A32
- Romano, D., Matteucci, F., Salucci, P., Chiappini, C., 2000, *ApJ*, 539, 235
- Sánchez, S. F., Galbany, L., Pérez, E., et al. 2015, *A&A*, 573, A105
- Sánchez-Menguiano, L., Sánchez, S. F., Kawata, D., et al., 2016, *ApJL*, 830, L40
- Sellwood, J. A., & Carlberg, R. G. 2014, *ApJ*, 785, 137
- Schmidt, M. 1959, *ApJ*, 129, 243
- Siebert, A., Famaey, B., Binney, J., et al., 2012, *MNRAS*, 425, 2335
- Silva Aguirre, V., Bojsen-Hansen, M., Slumstrup, D., et al. 2018, *MNRAS*, 475, 5487
- Spitoni, E., Gioannini, L., & Matteucci, F. 2017, *A&A*, 605, A38
- Spitoni E., Matteucci F., 2011, *A&A*, 531, A72
- Spitoni, E., Matteucci, F., Jönsson, H., Ryde, N., Romano, D. 2018, *A&A*, 612, A16
- Spitoni, E., Matteucci, F., Sozzetti, A., 2014, *MNRAS*, 440, 2588
- Spitoni, E., Recchi, S., Matteucci, F. 2008, *A&A*, 484, 743
- Spitoni, E., Romano, D., Matteucci, F., Ciotti, L., 2015, *ApJ*, 802, 129

- Spitoni, E., Silva Aguirre, V., Matteucci, F., Calura, F., & Grisoni, V., 2019, A&A, 623, A60
- van den Hoek, L. B., Groenewegen, M. A. T. 1997, A&AS., 123, 305
- Vincenzo, F., Spitoni, E., Calura, F., et al., 2019, arXiv:1903.03465
- Vogt, F. P. A., Pérez, E., Dopita, M. A., Verdes-Montenegro, L., Borthakur, S., 2017, A&A, 601, A61
- Woosley, S. E., & Weaver, T. A. 1995, ApJ, 101, 181
- Zaritsky, D., & Rix, H.-W., 1997, ApJ, 477, 118